

01 Oct 2022

Effect of Cu Additions on Scale Structure and Descaling Efficiency of Low C Steel Reheated in a Combustion Gas Atmosphere

Richard Osei

Simon Lekakh

Missouri University of Science and Technology, lekakhs@mst.edu

Ronald J. O'Malley

Missouri University of Science and Technology, omalleyr@mst.edu

Follow this and additional works at: https://scholarsmine.mst.edu/matsci_eng_facwork



Part of the [Materials Science and Engineering Commons](#)

Recommended Citation

R. Osei et al., "Effect of Cu Additions on Scale Structure and Descaling Efficiency of Low C Steel Reheated in a Combustion Gas Atmosphere," *Oxidation of Metals*, vol. 98, no. 3 thru 4, pp. 363 - 383, Springer, Oct 2022.

The definitive version is available at <https://doi.org/10.1007/s11085-022-10125-3>

This Article - Journal is brought to you for free and open access by Scholars' Mine. It has been accepted for inclusion in Materials Science and Engineering Faculty Research & Creative Works by an authorized administrator of Scholars' Mine. This work is protected by U. S. Copyright Law. Unauthorized use including reproduction for redistribution requires the permission of the copyright holder. For more information, please contact scholarsmine@mst.edu.



Effect of Cu Additions on Scale Structure and Descaling Efficiency of Low C Steel Reheated in a Combustion Gas Atmosphere

Richard Osei¹ · Simon Lekakh¹ · Ronald O'Malley¹

Received: 9 February 2022 / Revised: 10 July 2022 / Accepted: 18 July 2022 /

Published online: 13 August 2022

© The Author(s) 2022

Abstract

Modern EAF steelmaking employs scrap as its primary source of raw material. Different sources of scrap have varying levels of residuals, which can negatively influence product properties, performance, and surface quality. The presence of some residuals, such as Cu and Ni in controlled quantities, can also positively impact steel performance for some applications. It is also well known that interactions between residuals and alloying elements in steel can modify the structure of scale formed during slab reheating prior to hot rolling. These changes in the scale structure can influence scale removability. In this study, the effect of varying Cu concentrations in a low alloyed Mn and Si containing steel was examined to investigate its impact on scale removability. Laboratory studies were performed with simulated reheating and descaling conditions that mimic the conditions used in industrial practices. The scale structure that formed during reheating in the combustion atmosphere was investigated using SEM/EDX analysis. A special laboratory water jet descaling device was used to evaluate scale removability at three different hydraulic impact factors. The results showed that Cu at different levels significantly modified scale structure that formed, particularly the internal scale layers, which affected scale removability at different applied descaling impact factors. The effects of Cu level and descaling impact factor on scale removability is discussed.

Keywords Reheating · Cu-enrichment · Descaling · Scale structure · Impact factor

✉ Richard Osei
rovhb@umsystem.edu

¹ Department of Materials Science and Engineering, Peaslee Steel Manufacturing Research Center, Missouri University of Science and Technology, Rolla, MO 65409, USA

Introduction

Steel production has evolved through the nineteenth century to the twenty-first century with raw materials increasingly switching from primarily pig iron to scrap [1–3]. Today in the US, over 70% of the steel is produced in the electric arc furnace (EAFs) using large proportions of recycled steel scrap as the primary charge material due to its economic advantages and environmental friendliness [4, 5]. However, scrap melting to produce steel has a major challenge due to the accumulation of high levels of residuals in the continually recycled scrap stream [6, 7]. These residuals in scrap (Cu, Ni, Sn, Sb, Pb, As) remain in the steel during the steelmaking process because they cannot be preferentially oxidized and captured in the slag phase during melting [8]. The presence of these residual causes' challenges in the downstream processing of the steel. A commonly known residual is Cu, which has been reported to be present in the highest amounts and poses significant challenge in steel manufacture [6, 7, 9]. Even though some studies have shown that Cu can improve the corrosion resistance and increase the strength of steel [10–13], its presence often causes problems during mechanical working at high temperatures, a phenomena know as Cu surface hot shortness in steels [7, 14–16].

The surface hot shortness phenomena have been examined intensively in various studies to explain the mechanisms of damage [17–21]. Cu hot short defects are most commonly observed in downstream processes such as reheating, and hot rolling of slabs or the forming of steel products. During reheating, the cast slab surface is exposed to a complex, oxidizing combustion gas atmosphere (CO_2 , O_2 , H_2O , N_2) at temperatures above 1100 °C. During such reheating, iron Fe readily oxidized to form scale. Cu having a limited solubility in solid iron and a low affinity for oxide formation gets enriched at the oxide/metal interface as the Fe oxidizes. The enrichment of Cu at the oxide/metal interface rapidly reaches saturation and forms a liquid phase due its low melting point at 1085 °C. The Cu-liquid phase then wets and penetrates the austenite grain boundaries, leading to liquid embrittlement and providing a path for oxygen penetration which causes cracking during hot rolling [15]. The presence of surface cracks is undesirable in steelmaking. Different approaches have been adopted to suppress this defects in steel. Most steel producers' resort to metallic charge management to control Cu levels in steel by using low residual scrap and blending with virgin iron units such as direct reduced iron (DRI) or pig iron to dilute Cu levels in liquid steel. Another suggested approach is the addition of Ni to increase the melting point of the precipitated Cu-Ni phase so that it exceeds the reheating temperature and liquid is avoided. In addition, Ni also increases the solubility of Cu in austenite [22, 23]. Other studies have reported that, reheating of slabs at extreme temperatures above 1200 °C decreased surface hot shortness [21]. However, it has been reported that the presence of tramp elements like Sn in low amounts up to 0.04 wt% increases the severity of surface hot shortness by decreasing the solubility of Cu at reheating temperatures in austenite. This occurs by lowering the melting temperature of the precipitated Cu-Sn phase [21, 23], thereby decreasing the temperature at which liquid can form and austenite grain boundary wetting can occur.

Most studies on residual Cu in steel have been focused on reheating, and mechanical deformation by hot rolling to report the mechanisms and effects associated with Cu residuals in steels. However, a critical intermediate descaling step between reheating and hot rolling has not been fully investigated. This descaling step involves the removal of the scale that forms on slabs during reheating, generally by hydraulic decaling means using water pressures as high as 4000 psi (27.58 MPa). This process is a critical step which helps to improve surface quality of rolled steel and reduces defect formations associated with rolled-in scale. The descaling step may be carried out in different stages: primary and secondary with 3 or more descaling steps in extreme cases for certain steel grades. The major challenge associated with scale removal by descaling can be grouped into three factors: (i) oxide structure (steel chemistry), (ii) nozzle design, and (iii) hydraulic parameters [24–28]. In the case of steel chemistry, reports [29] have shown how different elements present in steel (C, Mn, Si) influences the structure of the oxide scale, particularly in the subsurface region, and its corresponding effect on scale removability. Residual elements like Ni have also been reported to modify the structure of the oxide/steel interface, increasing unevenness, and decreasing scale removability [7, 30]. However, Cu residuals, known to cause surface hot shortness in steel, has not been investigated in relation to its effect on scale removability and this knowledge could be important to steel producers.

The objective of this study was to evaluate the effect of different levels of Cu in a low carbon steel on the scale structure that forms during reheating and its effect on scale removal efficiency. Industrial reheating conditions in a combustion gas atmosphere was simulated in the laboratory for scale formation, followed by descaling using a specially designed high precision CNC descaling device that allows descaling with varying impact factor to be performed.

Experimental Procedures

The composition of the steels used in this study are presented in Table 1 with their average grain size after casting. This set of laboratory cast low carbon steels varied in Cu content, which were labeled as low, medium, and high Cu. The steel chemistries after laboratory casting were reported by OES and Leco analysis. The cast plates were carefully machined to 165 mm × 110 mm × 20 mm rectangular samples to remove the cast surface. Machined samples were finished using wet grinding with 60 grit silicon carbide and the surface quality of the ground sample was measured to have Ra of 0.271 μm using 3D optical profiler (Nanovea, Model

Table 1 Lab cast steels used in this work (wt%)

Steel	C	Si	Mn	Cu	Grain size (μm)
Low Cu	0.13	0.30	0.36	0.24	66 ± 16
Medium Cu	0.11	0.28	0.34	0.54	62 ± 12
High Cu	0.13	0.29	0.33	0.80	75 ± 23

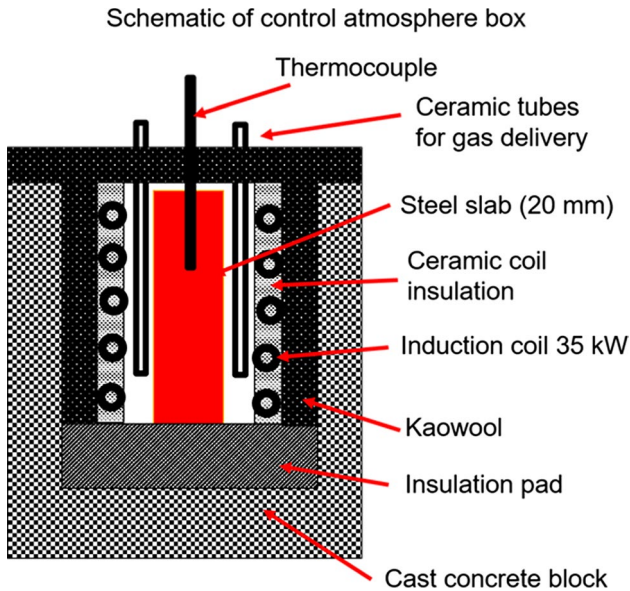


Fig. 1 Induction furnace for reheating steel slab in a controlled atmosphere

Table 2 Reheating industrial conditions, which were simulated in laboratory tests

Combustion gas (vol%)	Temperature (°C)	Time (min)
8.5 CO ₂ , 17 H ₂ O, 2 O ₂ , N ₂ bal	1200	90

PS50 Micro Photonic Inc.) [29]. To prevent rusting prior to testing, sample surfaces were preserved by cleaning with ethanol and air drying.

To simulate industrial scale formation during reheating, the samples were reheated in a 35kw induction melting furnace (Model LSZ-35), having a 200 mm × 130 mm × 25 mm induction chamber, which was embedded in an enclosure to allow for control of the furnace atmosphere (Fig. 1). The atmosphere of the industrial reheating furnace was simulated by mixing gases in proportions that reproduced the natural gas combustion atmosphere in an industrial furnace (Table 2). An excess oxygen level of 2% was chosen for this study based on observed industrial reheat furnace operating conditions. The gas flow rate supplied to the heating chamber was 6000 ml/min, which provided approximately a 2 cm/sec gas velocity in the reaction zone [29]. Calculations confirmed the absence of gas starvation in the reaction zone at this flowrate. The temperature during reheating was controlled by a K-type thermocouple inserted into the slab. The thermocouple enabled adjustment of the furnace power to control the reheating temperature within ± 10 °C. The reheating temperature and time employed for the test was 1200 °C for 90 min, which is typical for soak zones temperatures and residence times in industrial reheat furnaces.

At the end of the reheating period, the sample was carefully removed from the furnace chamber and quickly transported into a descaling chamber to minimize cooling prior to descaling. The hot sample was subjected to hydraulic descaling using high pressurized water. A CNC stage setup was used for descaling (Fig. 2) that allowed the standoff distance from the sample surface to the nozzle to be varied during the descaling process. A detailed description of the setup used was provided in a previously published article [29]. This approach allowed descaling to be conducted at different spray heights which corresponded to different Impact Factors (IF) (N/mm^2). The descaling was conducted at a spray lead angle of 15° at a flowrate of 4 gpm (15.14 lpm) at 4000 psi (27.58 MPa) and at a speed of 0.01 m/s. The standoff distance Z between the spray nozzle and the slab surface was programmed to vary across the length of the slab by decreasing the height of the spray nozzle to cause a corresponding increase in IF. The experimental IF relating to nozzle position was verified using pressure gauges at a sponsor's facility (Spray System Inc.) [29] and designated in this article as "low IF" for $1 \text{ N}/\text{mm}^2$, "medium IF" for $1.4 \text{ N}/\text{mm}^2$, and "high IF" for $2.2 \text{ N}/\text{mm}^2$. After descaling, the plate was quenched with cold water to prevent the development of secondary scale. The three footprint areas formed during descaling with varying IF (Fig. 2c) were coated with epoxy to preserve the surface for subsequent examination. Due to the hot charged descaling practice used in this study which required the sample to be descaled immediately after the reheating cycle, oxidized specimen could not be measured for mass change, but instead cross-sectional SEM analysis was used to determine scale growth from oxide thickness measurements.

After the descaling experiment, a Maxiém CNC waterjet with fine abrasive (Model OMAX 0707) was used to extract rectangular $10 \text{ mm} \times 15 \text{ mm} \times 20 \text{ mm}$ samples from the different footprint zones along the length of the sample. A sample with the original formed scale was also extracted from the non-descaled part of the reheated slab for analysis. All extracted samples were cross-sectioned with high precision wet abrasive cutting slow speed saw, mounted in epoxy, ground using silicon carbide abrasive papers to 1200 grit and mechanically polished with $0.1 \mu\text{m}$ diamond paste using low polishing pressure to minimize scale breakage. The morphology, thickness, microstructure, and chemistry of the original and residual oxide layers were analyzed with a scanning electron microscope (SEM TESCAN-ASCAT system equipped with Bruker energy dispersive spectroscopy (EDX). HORIBA Jobin-Yvon Raman spectroscopy (LabRam ARAMIS) was also used to identify the oxide phases that were present and compared to reported phases in RRUFF database [31]. A quantitative approach was used to evaluate the descaling efficiency by classifying the descaled surfaces into 3 categories of residual scale structures and measuring the percentages of each structure on cross-sectioned samples extracted from the descaled footprint. The quantification was done for the entire width of the extracted descaled area (15 mm) by taking SEM images between 20 and 40 frames at a magnification of $100 \mu\text{m}$. ImageJ software was used as a measuring tool to quantify the 3 different surface classes.

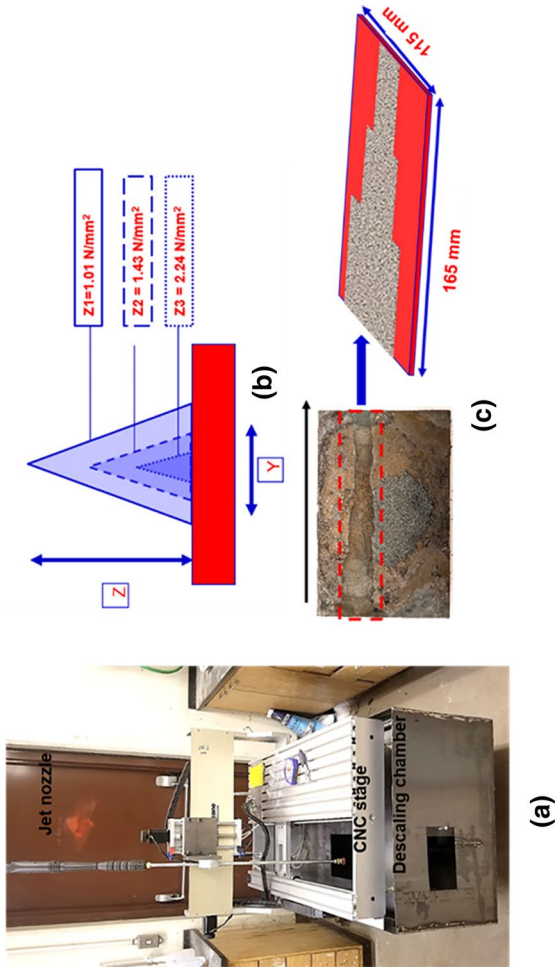


Fig. 2 Descaling setup using a CNC stage: **a** CNC stage with jet nozzle, **b** variation in impact factor, and **c** footprint of descaled slab

Results and Discussion

Characterization of Scale Formed During Reheating

Low Cu Steel

Figure 3 shows the cross-sectional microstructure of the scale that formed on the low Cu steel (Table 1) oxidized at 1200 °C for 90 min in a combustion gas atmosphere. The scale structure consisted of several distinguishing layers. A dense *external layer* with average thickness of $776 \pm 134 \mu\text{m}$. This external layer had random long transverse cracks running on the middle of this layer and also lateral cracks running through the whole thickness of this layer. Void formation was observed to be

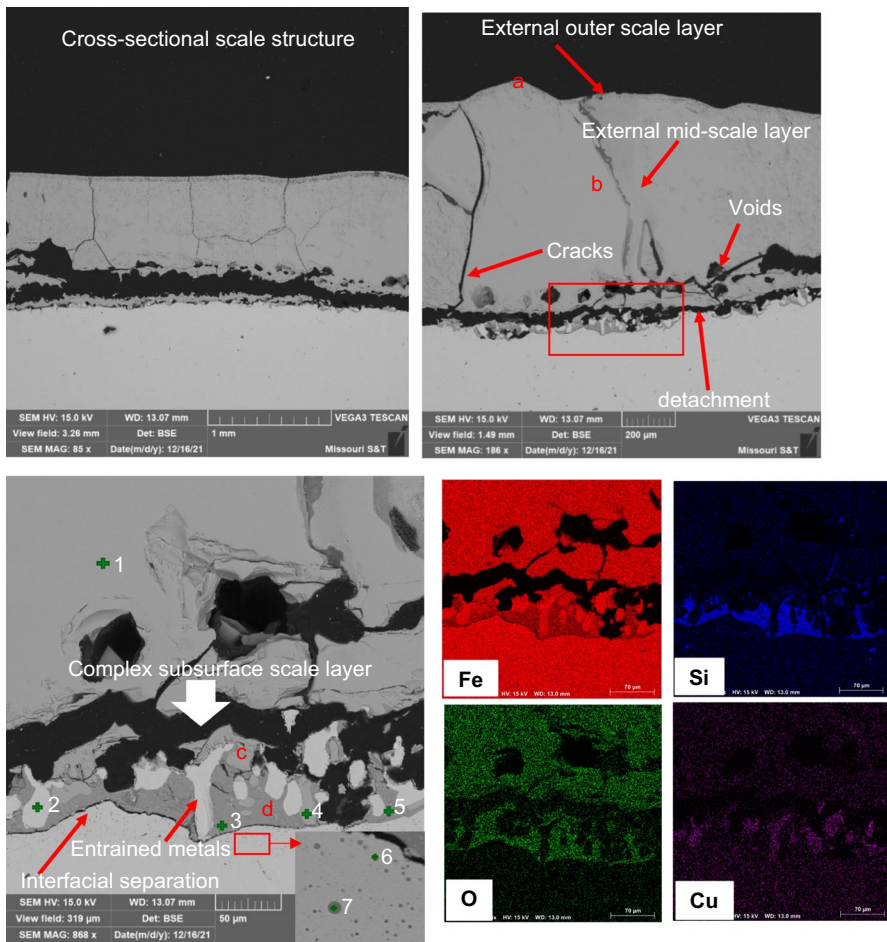


Fig. 3 Cross-sectional BSE image of scale structure for low Cu steel: top-left (low magnification), top-right (medium magnification), bottom-left (high-magnification), and bottom-right (EDX elemental map)

predominant at the bottom of the external scale layer, close to what can be described as complex internal/subsurface layer, which will be referred in this article as the *subsurface layer*. The complex subsurface layer was measured to be $50 \pm 19 \mu\text{m}$ in average scale thickness. There was significant detachment, separating the external scale layer from the complex subsurface layer visible in many sections. However, a strong attachment of these two layers were also observed in some sections. The interface between the external scale and subsurface structure contained pores and was structurally uneven.

The subsurface structure contained scattered entrainment of metals having different sizes and orientations. EDX mapping of the scale structure showed the distribution of elements making up the different oxide phases in the scale structure. EDX chemistry analysis of the oxide scale (Table 3) revealed that the external scale layer contained Fe oxide with trace presence of Mn and Ni. The complex subsurface contained a mixed chemistry of metallic Fe with trace of Cu *in entrained islands*, Fe-based oxides and Fe-Si based oxides with trace presence of Mn. Actually, in the reheated low Cu steel, Cu seemed to stay in solid solution in different oxide phases rather than to be present as separate high concentration precipitate. A randomly scattered dotted layer in the steel matrix beneath the subsurface layer contained micro diameter pockets of oxides. These tiny precipitates were formed internally and were superimposed on the metal substrate, extending about $40 \mu\text{m}$ deep from the oxide/metal interface. The chemistry of that near spherical precipitates showed a presence of a mixed Fe–Si–Mn based oxides with a range of Si presence. Phase identification using Raman spectroscopy revealed the external scale to contain Fe_2O_3 and Fe_3O_4 phases, with the Fe_2O_3 located at the outer part of the external scale (about $5 \mu\text{m}$) and the Fe_3O_4 located just below that layer through to the mid external scale (Fig. 4). The complex subsurface layer contained mainly a mixture of two phases: Fe_2SiO_4 and Fe_3O_4 .

Medium Cu Steel

The cross-sectional investigation of the reheated medium Cu steel (Fig. 5) revealed some similarity and also some detectable differences in scale structure when compared to low Cu steel. In both cases, scale consisted of external layer and a merged

Table 3 Oxide scale composition of low Cu steel (wt%)

Point	Fe	O	Si	Mn	Cr	Ni	Cu
1	77.0	22.2	–	0.4	–	0.4	–
2	93.6	–	–	–	–	–	6.4
3	63.2	27.5	7.9	1.0	–	0.4	–
4	77.2	22.3	–	0.5	–	–	–
5	59.9	27.2	8.4	1.0	–	0.5	3.0
6	56.5	26.0	5.4	11.3	0.8	–	–
7	29.6	29.2	10.3	30.0	0.5	0.4	–

Points are from Fig. 3

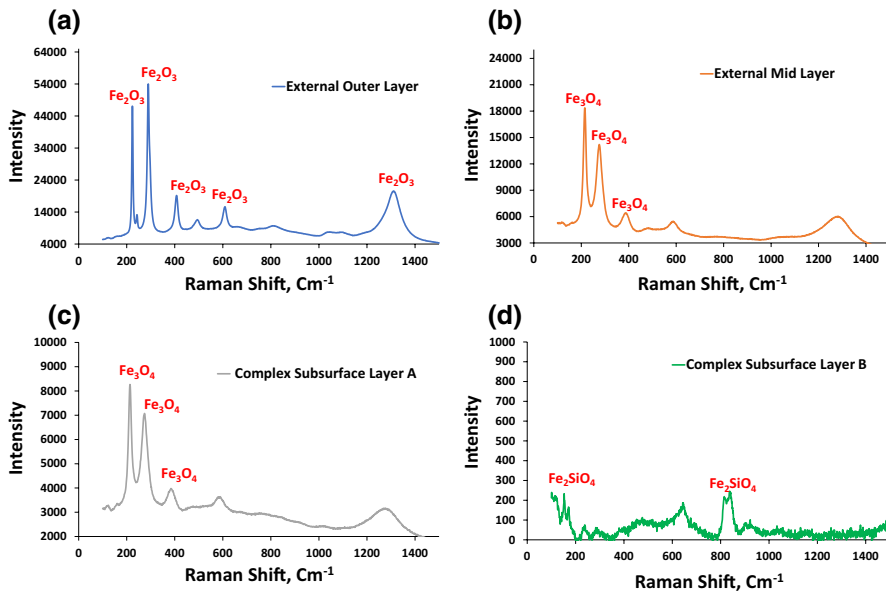


Fig. 4 Phases identified in scale using Raman spectroscopy: **a** phases in external outer layer, **b** phases in external mid-scale layer, and phases in complex subsurface layer: **c** in point #4, Fig. 3, and **d** in point #5, Fig. 3

external/complex subsurface layer. The external scale layer with average thickness measuring $411 \pm 93 \mu\text{m}$ was dense with few internal defects and had vertical cracks. Also, a lateral crack separated a portion of the external layer from the merged external/complex subsurface scale layer. In many spots, a lower portion of external layer was merged with subsurface layer forming complex external/subsurface scale layer which measured between $83 \pm 16 \mu\text{m}$ in average scale thickness. A few defects in this complex scale structure contained pores with randomly scattered metal entrainment. The merged external/complex subsurface scale structure appeared to be adherent to the metal substrate with few sections showing partial detachments.

Analysis of the merged external/complex subsurface layer revealed two different types of oxide formations close to the substrate. The first type of oxide formation exhibited 3 layered phases: the first was an iron oxide layer followed by a fayalite layer, and finally by another iron oxide layer. This last bottom iron oxide layer exhibited interfacial separation from the steel matrix in some sections and was bonded to the steel matrix by an enriched liquid Cu layer in other sections. The second oxide formation also revealed 3 layered phases: a continuous iron oxide layer about $80 \mu\text{m}$ in thickness (stemming from the external layer), followed by a eutectic fayalite oxide phase with precipitates of iron oxide (complex subsurface), and finally an enriched liquid Cu phase beneath it just on metal matrix boundary. This structure appeared to be strongly adhered to the metal substrate due to the presence of possibly two liquid phases (eutectic fayalite and liquid Cu) at the reheating temperature.

EDX chemistry analysis of the oxide scale (Table 4 in points shown in Fig. 5) revealed that the external scale layer contained iron oxide with trace presence of

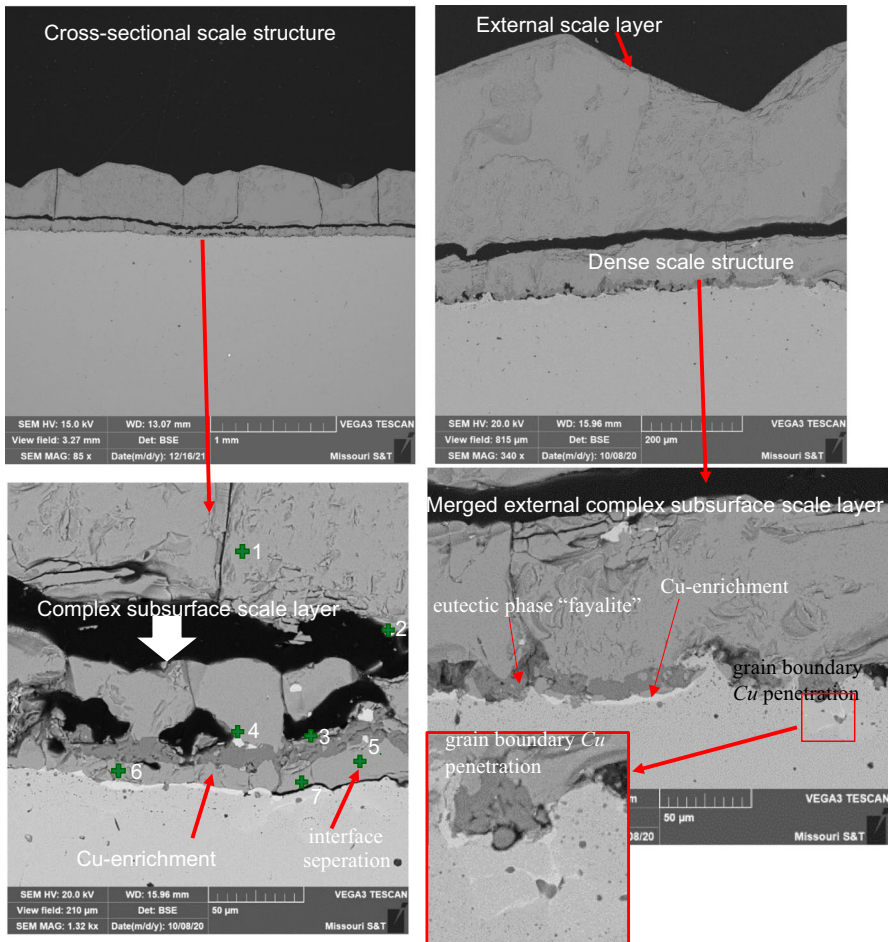


Fig. 5 Cross-sectional BSE image of scale structure for medium Cu steel: top-left (low magnification), top-right (medium magnification). Bottom-left and right (high-magnifications) illustrated second oxide structure bonded to the matrix

Table 4 Oxide scale composition of medium Cu steel (wt%)

Point	Fe	O	Si	Mn	Cr	Ni	Cu
1	77.2	22.3	–	0.4	–	–	–
2	13.9	–	–	–	–	–	85.1
3	61.3	28.2	9.0	1.0	–	–	–
4	6.4	–	–	–	–	0.7	92.4
5	76.4	22.3	–	0.5	0.3	0.3	–
6	6.2	–	–	–	–	0.8	92.7
7	55.8	27.2	7.7	6.6	–	0.4	1.7

Points are from Fig. 5

Mn. Phase identification revealed the external scale to contain Fe_2O_3 and Fe_3O_4 phases. The merged external/complex subsurface layer contained a mixed chemistry of Cu-Fe metal entrainment in the scale structure, Fe-based oxides and Fe-Si based oxides with trace presence of Mn. Phase identification revealed this layer to be a mixed phase of Fe_2SiO_4 and Fe_3O_4 . Possible mechanisms responsible for such complex oxide structural variations and formations are unknown at this point. Further studies are required to fully understand the mechanisms responsible for this type of formation. These structural differences in the low and medium Cu alloyed steels could affect descaling efficiency which will be discussed in the next section of this paper.

High Cu Steel

The scale formed in reheated high Cu steel (Fig. 6) was characterized by larger defects in the external scale layers (gaps and voids), transverse cracks and metallic precipitation in the scale structure. The external scale measured between $752 \pm 93 \mu\text{m}$ in average scale thickness. The defects were non-uniform throughout the scale structure, with some sections showing consistent dense morphology. The external scale layer was laterally separated from the complex subsurface scale layer. The voids in the external scale layer increased inward the external scale structure, close to the external/complex subsurface layer boundary. The complex subsurface scale layer was significantly different compared to the other lower Cu steel samples. It had a lower average scale thickness ($31 \pm 17 \mu\text{m}$). The complex subsurface layer was characterized by massive Cu precipitation and enrichment at the oxide/metal interface with high unevenness. Few sections were observed to have complex oxides formations. The massive liquid Cu phase might have restricted the rapid formation of the complex subsurface oxides when compared to the low and medium Cu steels, leading to its lower thickness at the metal interface. However, a much deeper penetration of pure Cu-phase, up to about $100 \mu\text{m}$ along the austenite grains boundaries was observed in the high Cu steel. EDX chemistry analysis (Table 5) of the oxide scale revealed the external scale layer to contain iron oxide with trace presence of Mn and entrainment of Cu metal having trace presence of Fe. The complex subsurface oxide layer contained a mixed chemistry of Cu-Fe metal entrainment in the scale structure, Fe-based oxides, and Fe-Si based oxides (fayalite) with trace presence of Mn and Al. Elemental mapping showed the distribution of elements in the scale structure at the boundary between the external and complex subsurface (Fig. 6).

Table 6 summarized findings of the thicknesses of the scale layers formed during reheating of different Cu-alloyed steels. There was no general trend, which indicated that multiple mechanisms were at play that were affected by Cu addition. Liquid Cu films at the scale/matrix interface appeared to promote the formation of a thicker and more complex merged internal/subsurface layer in the medium Cu steel. However, continuous, and deep penetration into the austenite grain boundary by the liquid Cu film could possibly have suppressed diffusion limited oxidation process and decreased the thickness of subsurface layer. More importantly, from the standpoint of descaling efficiency, a dominant factor could be changes in adhesion

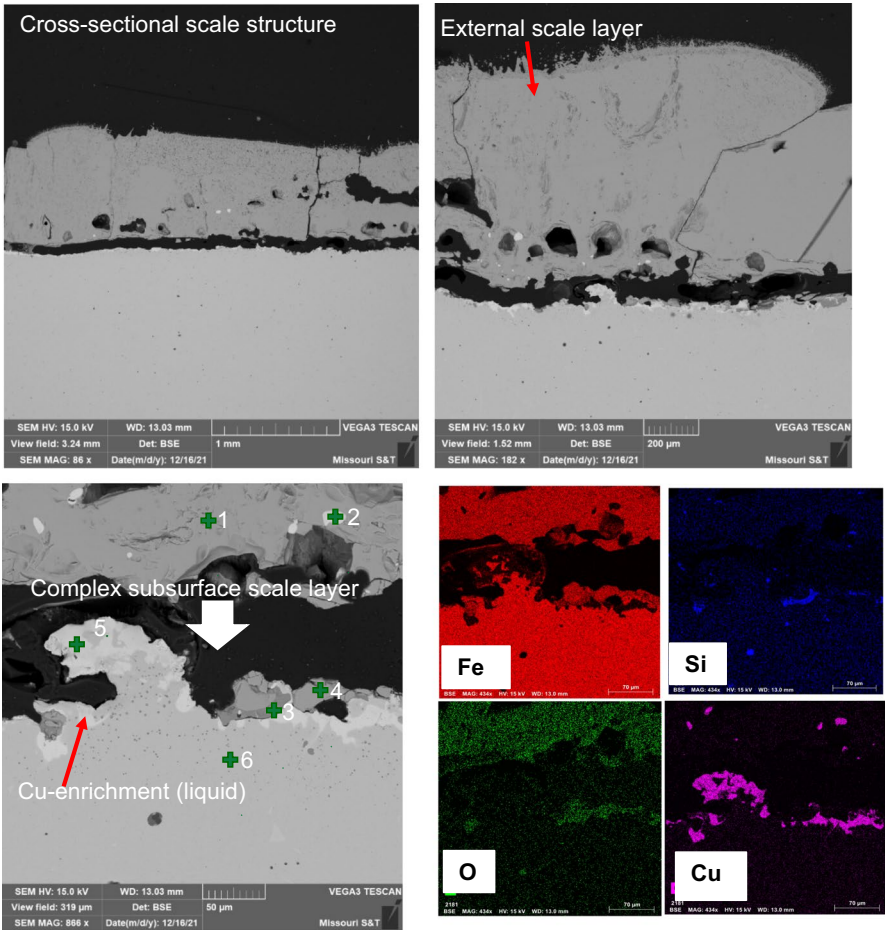


Fig. 6 Cross-sectional BSE image of scale structure for high Cu steel: top-left (low magnification), top-right (medium magnification), bottom-left (high-magnification), and bottom-right (elemental map)

Table 5 Oxide scale composition of high Cu steel (wt%)

Point	Fe	O	Si	Mn	Cr	Al	Ni	Cu
1	76.6	22.3	–	0.5	–	–	–	–
2	4.3	–	–	–	–	–	–	95.7
3	61.7	28.0	8.7	1.0	–	–	–	0.6
4	76.8	22.3	–	0.3	–	–	–	–
5	5.9	–	–	–	–	–	–	94.1
6	34.4	32.2	14.3	17.8	–	0.9	–	–

Points are from Fig. 6

Table 6 Comparison of average scale thickness (μm) and structure of complex internal/subsurface layer

Steel	External	Complex subsurface	Structure description
Low Cu	776 ± 134	50 ± 19	Scattered metal entrainment in mixed iron oxide/fayalite phase
Medium Cu	411 ± 93	83 ± 16	Two layered oxide formation: (i) iron oxide/fayalite/iron oxide (interfacial separation), and (ii), iron oxide/fayalite/Cu-enrichment (strong adherence to substrate)
High Cu	752 ± 93	31 ± 17	Massive Cu-enrichment with deep grain boundary penetration, restricted complex oxide formation

between oxide and metal matrix, which will be investigated by varying water jet impact factor.

Descaling Efficiency

Classification of Descaled Surface Quality

Reheated steels were subjected to water jet descaling with variations in the impact factor (IF). To obtain quantitative data from these experiments, the quality of the descaled surfaces was grouped into three surfaces classes (Fig. 7):

- class A had a completely removed external and complex subsurface oxides;
- class B had a completely removed external layer and partially removed complex subsurface scale layer, (with presence of the residual Fe_2SiO_4 phase); and
- class C had completely removed external layer and some complex subsurface (Fe_2SiO_4) but contained penetrating oxide with root-like scale structure having metal entrainment.

Low Cu Steel

After reheating of the low Cu steel, the oxidized sample followed a hot charge descaling schedule on a CNC stage that was programmed to produce three varied

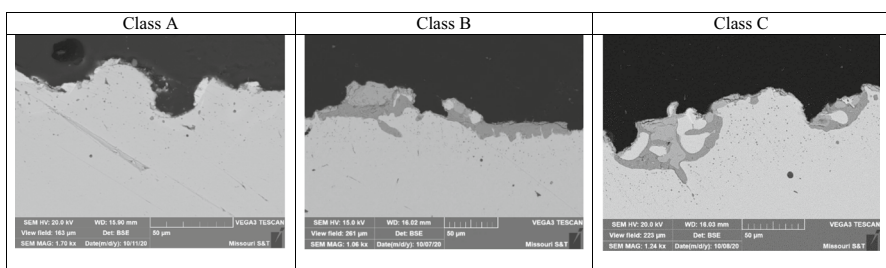


Fig. 7 Descaled surface quality classification

standoff distances to cause a corresponding change in applied nozzle impact factor (IF). After descaling, samples were extracted from the regions with different nozzle footprints and analyzed to quantify descaling efficiency. Analysis and quantification of the surface quality using the criteria described above showed significant difference in descaling efficiency when the impact factor (IF) was varied from low to high. Figure 8 illustrates a typical residual scale condition after descaling with different IF and the actual averaged percentage each of the three categories (A, B, and C) of surface quality. The quantified results showed that, the low IF condition resulted in complete removal of the external scale (Fe-oxides) and partial removal of the internal scale (mixed Fe–Si based oxides), accounting for up to 61% clean surface for class A and 39% residual scale (23% class B and 16% C). The residual scale thickness at the first stage measured $18 \pm 8 \mu\text{m}$ and $12 \pm 2 \mu\text{m}$ for surface class B and C respectively. The residual scales were characterized by deep penetrating oxide roots up to about $40 \mu\text{m}$ into the metal matrix from the oxide/metal boundary as well as complex orientations for these oxide, particularly for that of surface class C. When IF was increased to the medium

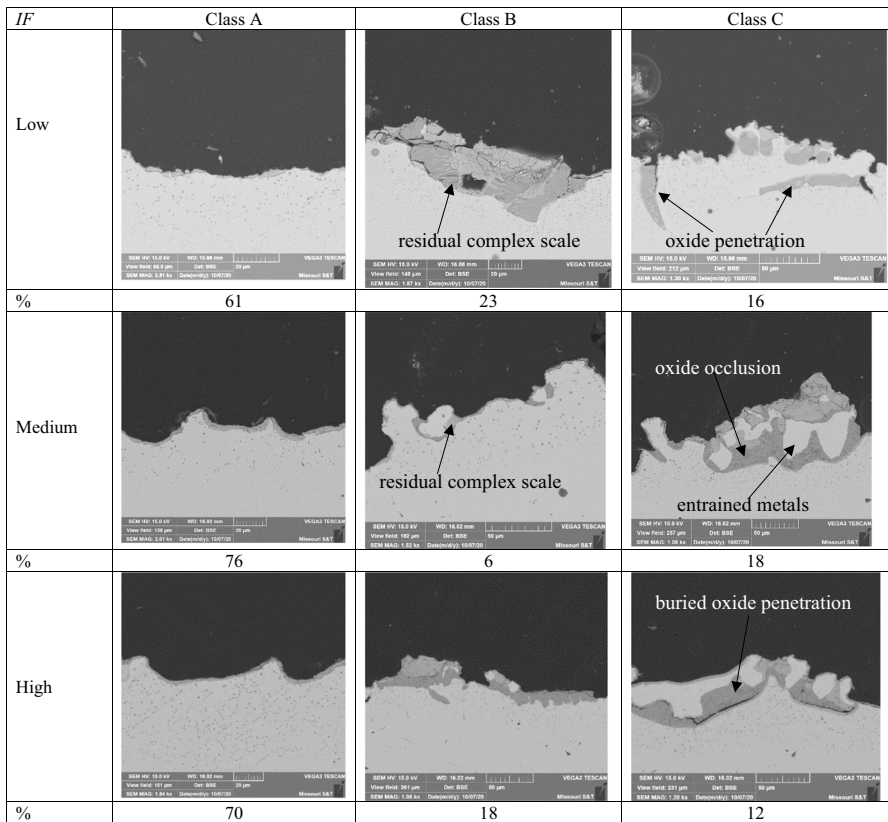


Fig. 8 Quantified surface quality of low Cu steel after descaling at different IF

condition, there was a corresponding increasing in the clean surface class A from initial 61% to 76%, which reflected a decrease in the overall residual scale (class B plus C) from 39 to 24%. The residual scale class B reported the highest reduction, from 23 to 6%. The residual scale thickness in class B decreased to 7 ± 3 μm while class C measured 46 ± 12 μm . The residual class C scale was characterized as oxides with entrained metal as well as oxide formation beneath the cluster of entrained metal which appeared to be occluded. The original scale analysis reported higher scale thicknesses in the subsurface sections having higher metal entrainment due to their larger size. This resulted in the decreasing class B and some redistribution of residual scale between, classes B and C.

At the highest IF condition, there was no significant effect in total descaling efficiency (class A), while some reversal in different surface classes with residual scale were observed. At high IF, residual scale totaled 30%, having 18% class B and 12% class C respectively. These results once again highlight the non-uniformity in the formed original scale which likely resulted from complex mixed controlled oxidation mechanisms during the reheating process [32–35]. The residual class C scale was characterized by oxide buried beneath metal that stretched greater than 100 μm in length. Such scale structural formations may impede descaling since the formed oxides may not be in direct contact with the impinging water pressure from the nozzles during descaling. The residual scale thickness measured 8 ± 3 μm for class B and 37 ± 9 μm for class C.

Medium Cu Steel

Interestingly, there were no significant changes in descaling efficiency at the lower applied IF in medium Cu steel when compared to low Cu steel. However, significant effect was observed at high IF. In this case, a higher descaling efficiency, above 90% was achieved for the medium and high IF (Fig. 9). Specifically, at the low IF, only 52% of clean surface quality class A was quantified with 48% residual scale of both class B and C combined. The predominant residual scale was that of class B, accounting for 28% with what appeared to be residuals from the first type of oxide formation in the merged external/complex subsurface layer. The residual scale measured 15 ± 7 μm for class B and 22 ± 6 μm for class C which made up 20% of the total residual. At the medium applied IF, there was a significant increase in clean surface class A from initial 52% to 94%, with a rapid decrease in residual scale class B and C. Residual scale observed at the medium IF were mostly oxide penetration into the matrix from the interface with curved geometry bending down into the substrate. The measured residual scale exhibited a significant reduction in its thickness (9 ± 5 μm). Similar results were achieved at the highest applied IF condition: the quantified clean surface class A was near the same as for medium IF or about 90%. The residual scale at this conditions was 5% each for both class B and C surface quantifications. Strong evidence of *Cu-enrichment* was observed at this condition. The measured residual scale thickness was similar to that of the medium IF condition. The residual scale (class B and C) contained mixed phases of iron oxide, fayalite and iron oxide embedded in fayalite phase.

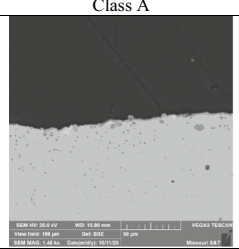
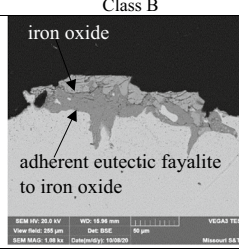
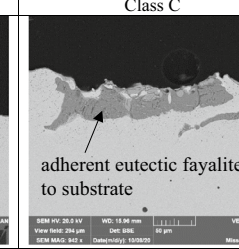
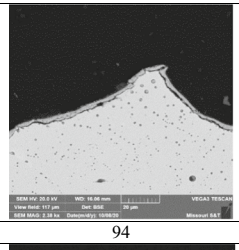
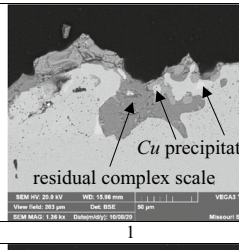
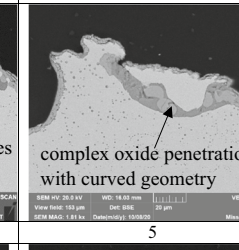
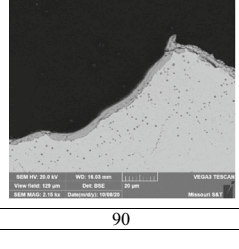
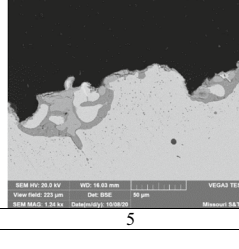
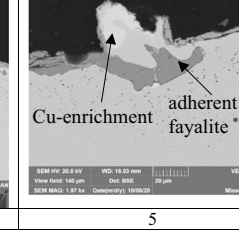
IF	Class A	Class B	Class C
Low			
%	52	28	20
Medium			
%	94	1	5
High			
%	90	5	5

Fig. 9 Quantified surface quality of medium Cu steel after descaling at different IF

High Cu Steel

In the high Cu steel, initial characterization of original scale structure prior to descaling saw a completely different internal scale layer structure, having liquid Cu-enrichment at the metal boundaries with complex oxide formation occurring randomly in few spots and sections (Fig. 6). The original complex subsurface oxide thickness measured $32 \pm 9 \mu\text{m}$. At the low IF condition, the descaling was highly efficient, with class A accounting for 98% (Fig. 10). The residual scale was less than 5%, having a thickness of $6 \pm 4 \mu\text{m}$. The residual scale was observed as penetrating roots at the interface where complex oxides had formed. The clean surface class A showed a strong presence of *Cu-enrichment* at the metal boundary. At the medium IF condition, there was no significant change in descaling efficiency quantified, the clean surface class A measured 97%. The residual scale class B which measured 1% was seen as complex oxide formations at sections with no Cu-enrichment ($7 \pm 3 \mu\text{m}$). The residual scale class C which measured 2% was observed as oxide formations in the Cu-enriched interface with penetration into the matrix. At the highest IF, the descaling efficiency was still above 90%. There was a small increase in residual scale (7%). The residual scale were

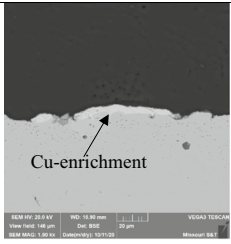
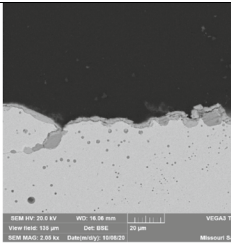
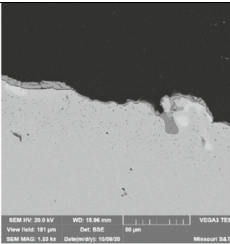
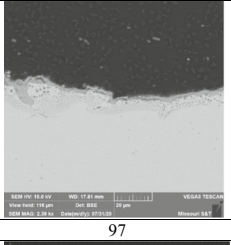
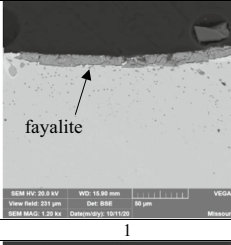
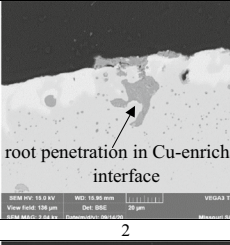
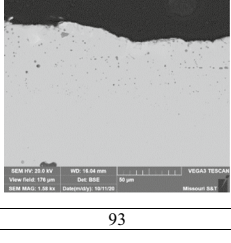
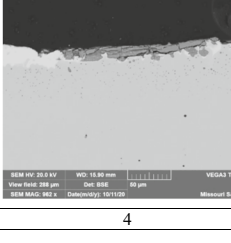
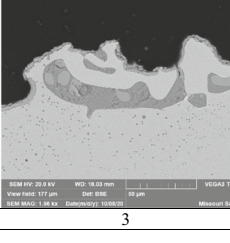
IF	Class A	Class B	Class C
Low			
%	98	1	1
Medium			
%	97	1	2
High			
%	93	4	3

Fig. 10 Quantified surface quality of high Cu steel after descaling at different IF

formations of fayalite phases (class B) at sections of the complex subsurface scale layer with little or no Cu-enrichment. These formations were observed as penetrations or superimposed oxides below the substrate interface with complex orientations and classified as class C. Residual scale thickness measured $8 \pm 3 \mu\text{m}$ for class B and $10 \pm 5 \mu\text{m}$ for class C.

Comparison of Descaling Efficiency in the Different Cu Steels

Comparison of descaling efficiency at varying IF in the different Cu steels is shown in Fig. 11. It was shown that the effective descaling of low Cu steel requires a higher IF than the maximum that was applied in this study (2.2 N/mm^2 IF) because only 70% descaling efficiency was achieved. It was observed that the high IF was just enough to remove the external layer and some complex subsurface oxide formations, but a significant amount of the complex oxide remained attached to the matrix after descaling. The probable cause of this result is related to the high level of metal entrainment in the complex scale layers of the low Cu steel. The presence of some entrained metal in the complex subsurface region also served as occlusion regions

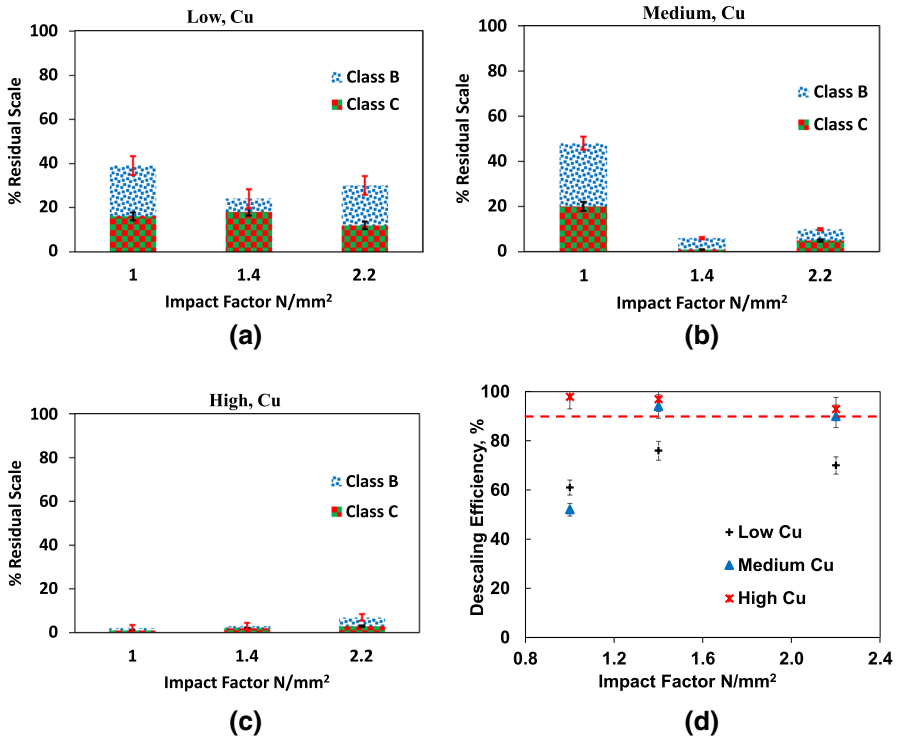


Fig. 11 Effect of IF and Cu in steel chemistry on descaling efficiency

for oxides as they formed within the crevices of metal clusters, which impeded its removal during descaling.

In the case of the medium Cu steel, the critical IF condition was between the medium and high levels (1.4–2.2 N/mm²) and it was enough to get a removal efficiency of 90% and above. At this Cu level in the steel, differences in the complex subsurface scale layer were observed after reheating, as well as a formation of liquid Cu phase. Cu enrichment in sections of the oxide/metal interface was also predominant in the microstructure. The two types of oxide formations observed could effect on adhesion to the matrix differently. The first type of layered oxide formation contained iron oxide/fayalite/iron oxide which might affect scale removability positively, while the second layered formation (iron oxide/fayalite) might impact scale removability negatively since it has been reported that scale structures having higher levels of fayalite presence at the oxide/metal interface respond poorly to descaling [29]. The Cu enriched liquid layer formed in medium Cu steel at reheating temperature decreased impact energy and promoted easier descaling at the medium IF. At the same time, from steel surface quality standpoint, deep Cu penetration into the austenite grain boundaries from the oxide/metal interface will lead to liquid embrittlement and cracking during hot rolling deformation [15].

The external/internal/subsurface modification in high Cu steel had dramatic effect on descaling efficiency. The results showed that the complex subsurface

scale layer was completely modified at this high Cu level. The scale layer contained fewer complex oxides formation at the oxide/metal interface and was occupied by liquid phase *Cu-enrichment* which impeded the formation of complex internal oxides as seen in its scale thickness measurements. In the high Cu steel, only a low critical impact factor (IF) was needed to achieve above 90% of scale removal.

In general, it was observed that Cu levels of 0.5 wt% and above, combined with medium IF conditions (1.4 N/mm^2) improved scale removal efficiency. Overall, the high Cu steel showed higher descaling efficiencies at all applied IF conditions. These results could be related to the decrease in complex subsurface oxide formation which might have been suppressed by liquefaction of Cu at the oxide/metal interface at reheating temperatures above the melting point of Cu ($1200 \text{ }^\circ\text{C} > 1085 \text{ }^\circ\text{C}$). Another possible explanation may be that the Cu phase was still liquid prior to descaling, hence enabling easy separation of the external and internal scale layer which was dominated by the presence of a Cu-enriched layer at the matrix interface.

Finally, all observations seen in the scale structures and their effect on descaling of the low carbon steels with different Cu levels are depicted schematically in Fig. 12. The phases present in the complex scale structures for the low carbon steels are identified in top part of this figure. The schematic depicts the scale structures after reheating and their transformation during descaling at varying impact factors.

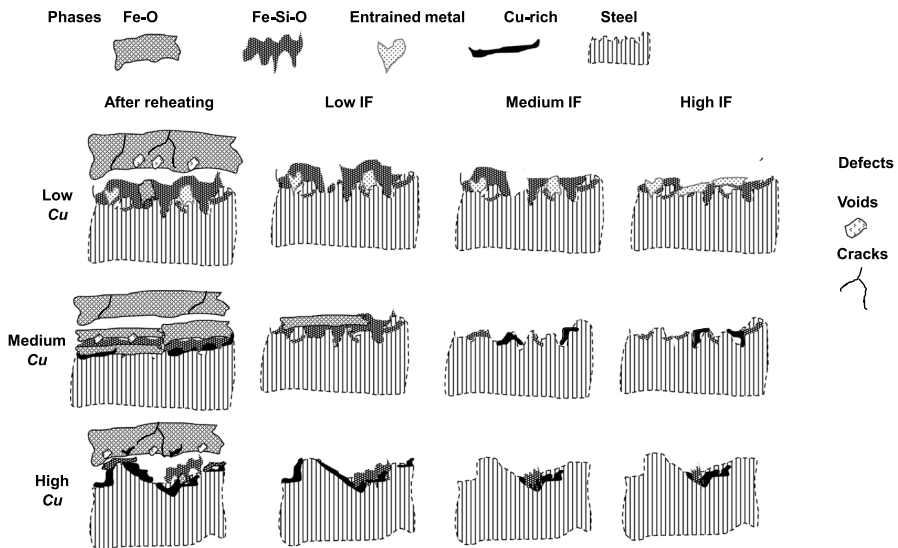


Fig. 12 Schematic representation of reheated scale structure of different Cu additions and its structural change during descaling at different impact factors

Conclusions

The effect of Cu additions in low carbon steels on scale formation during reheating and scale removal during descaling was investigated. The investigation was performed on 3 different Cu addition levels: low (0.2 wt%) medium (0.5 wt%) and high (0.8 wt%). At these different Cu additions, the oxide scale that formed during reheating in an oxidizing combustion gas atmosphere exhibited different structural properties, chemistries, and characteristics in the different scale layers (external and internal/complex subsurface) that formed. Major differences in the internal/complex subsurface scale layers close to the metal substrates were observed, which is critical for scale removal. Low Cu levels (0.2 wt%) exhibited random distribution of metallic Fe entrainment fused into the subsurface oxide structure which increased its complexity and strengthened its adhesion to the substrate. For the medium (0.5 wt%) and high (0.8 wt%) Cu level steels, the subsurface oxide contained less complexity with high *Cu-enrichment*, particularly the 0.8 wt% Cu steel, which exhibited a restricted complex subsurface development during reheating. The high Cu level steels (above 0.2 wt%) exhibited classic Cu penetration into the austenite grain boundaries of the steel from the enriched Cu liquid at the oxide/metal interface. This deep penetration appeared to suppress diffusion oxidation kinetics at the metal/oxide interface causing a decrease in subsurface scale growth and development.

The effect of Cu additions on the scale structure (subsurface) was evident during scale removal (descaling). The low Cu steel exhibited the lowest efficiency 70%, at high impact factor (IF) with the residual scale characterized by complex oxides (metallic Fe entrainment and oxide occlusions) that were strongly adherent to the metal substrate after descaling. The medium and high Cu steels exhibited improved descaling efficiency (above 90%) with less retained scale due to fewer complexities in the original subsurface oxides after reheating. The critical impact factor for efficient descaling of the low Cu addition was higher than the highest IF condition applied in this study ($> 2.2 \text{ N/mm}^2$), while the medium and high Cu additions required between 1.0 and 1.4 N/mm^2 IF for efficient descaling. This study demonstrated that increasing Cu additions decreased the complexity of the subsurface scale formed in low carbon steels which is critical for efficient descaling.

Acknowledgements This study is supported by Kent Peaslee Steel Manufacturing Research Center, and the authors gratefully acknowledges the support and guidance from the industry advisory committee of the PSMRC.

Open Access This article is licensed under a Creative Commons Attribution 4.0 International License, which permits use, sharing, adaptation, distribution and reproduction in any medium or format, as long as you give appropriate credit to the original author(s) and the source, provide a link to the Creative Commons licence, and indicate if changes were made. The images or other third party material in this article are included in the article's Creative Commons licence, unless indicated otherwise in a credit line to the material. If material is not included in the article's Creative Commons licence and your intended use is not permitted by statutory regulation or exceeds the permitted use, you will need to obtain permission directly from the copyright holder. To view a copy of this licence, visit <http://creativecommons.org/licenses/by/4.0/>.

References

1. R. J. Fruehan, in *The Making, Shaping and Treating of Steel: Steelmaking and Refining Volume* (1998), pp. 1–4.
2. T. Harada and H. Tanaka, *ISIJ International* **51**, 2011 (1301).
3. M. Xylia, S. Silveira, J. Duerinck, and F. Meinke-Hubeny, *Energy Efficiency* **11**, 2018 (1135).
4. J. A. T. Jones, B. Bowman, and P. A. Lefrank, in *Steelmaking and Refining Volume*, 11th edn. (The AISE Steel Foundation, Pittsburgh, 1998), pp. 525–660.
5. Energetics Inc.: Energy and Environmental Profile of the U.S. Iron and Steel Industry, DOE/EE-0229, United States Department of Energy, Office of Industrial Technologies, Washington, DC, 2000, pp. 10–26.
6. S. C. Marschman, On a Thermodynamic Approach to Material Selection for Service in Aggressive Multi-Component Gaseous and/or Vapor Environments, *Technical Report*, October 2015.
7. D. A. Melford, *Philosophical Transactions of the Royal Society London* **295**, 1980 (89).
8. B. Webler, L. Yin, and S. Sridhar, *Metallurgical and Materials Transactions B* **39B**, 2008 (725).
9. E. T. Stephenson, *Metallurgical Transactions A* **14A**, 1983 (343).
10. Y. W. Jang, J. H. Hong, and J. G. Kim, *Metals and Materials International* **15**, 2009 (623).
11. H. E. Townsend, *Corrosion* **57**, 2001 (497).
12. Z. B. Jiao, J. H. Luan, Z. W. Zhang, M. K. Miller, W. B. Ma, and C. T. Liu, *Acta Materialia* **61**, 2013 (5996).
13. S.-J. Kim, C. G. Lee, T.-H. Lee, and C.-S. Oh, *Scripta Materialia* **48**, 2003 (539).
14. M. I. Copeland and J. E. Kelley, *Bureau of Mines Report of Investigations* **7682**, 1972 (1).
15. A. Nicholson and J. D. Murray, *The Journal of the Iron and Steel Institute* **203**, 1965 (1007).
16. S. Koji, S. Soek-Jong, K. Masashi, U. Hiroshi, S. Akio, A. Kentaro, and C. Nagasaki, *Materials Transactions* **43**, 2002 (292).
17. G. Sahoo, M. Deepa, B. Singh, and A. Saxena, *Journal of Metals, Materials and Minerals* **26**, 2016 (1).
18. E. E. Glickman and M. Nathan, *Journal of Applied Physics* **85**, 1999 (3185).
19. M. G. Nicholas and C. F. Old, *Journal of Material Science* **14**, 1979 (1).
20. A. J. Hartley, P. Eastburn, and N. Leece, *Philosophical Transactions of the Royal Society of London. Series A, Mathematical and Physical Sciences* **295**, 1980 (45).
21. N. Imai, N. Komatsubara, and K. Kunishige, *ISIJ International* **37**, 1997 (217).
22. D. A. Melford, *The Journal of the Iron and Steel Institute* **200**, 1962 (290).
23. W. J. M. Salter, *The Journal of the Iron and Steel Institute* **204**, 1966 (478).
24. J. Frick, in *4th International Conference on Hydraulic Descaling* (London, 2003).
25. P. Lesli, in *AISTech 2005 Conference Proceedings* (2005).
26. J. W. Frick, *Metallurgical Plant and Technology International* **27**, 2004 (90).
27. M. Hnizdil and M. Raudensky, *Metals* **5**, 2010 (209).
28. H. Votavova and M. Pohanka, *Applied Mechanics and Materials* **821**, 2015 (152).
29. R. Osei, S.N. Lekakh, and R.J. O'Malley, P. Lesli, and S. Oldair, *Iron and Steel Technology* 48–59 (2021).
30. T. Asai, T. Soshiroda, and M. Miyahara, *ISIJ International* **37**, 1997 (272).
31. RRUFF spectral database, <https://rruff.info/>.
32. W. Kast and C.-R. Hohenthanner, *International Journal of Heat and Mass Transfer* **43**, 2000 (807).
33. H. F. Marston, P. H. Bolt, G. Leprince, M. Roder, R. Klima, J. Niska, and M. Jarl, *Iron and Steel Making* **31**, 2004 (57).
34. R. Osei, S.N. Lekakh, and R.J. O'Malley, in *AISTech 2020 Conference Proceedings*, 2020, pp. 1126–1137.
35. R. Osei, S. Lekakh, and R. O'Malley, *Metallurgical and Materials Transactions B* **52**, 2021 (3423).

Publisher's Note Springer Nature remains neutral with regard to jurisdictional claims in published maps and institutional affiliations.